Correlation effects in single–particle overlap functions and one–nucleon removal reactions

M.K. Gaidarov, K.A. Pavlova, S.S. Dimitrova, M.V. Stoitsov, and A.N. Antonov
Institute of Nuclear Research and Nuclear Energy, Bulgarian Academy of Sciences, Sofia 1784, Bulgaria

D. Van Neck
Laboratory for Theoretical Physics, Proeftuinstraat 86, B-9000 Gent, Belgium

H. Müther
Institut für Theoretische Physik, Universität Tübingen, Auf der Morgenstelle 14, D-72076 Tübingen, Germany

Single–particle overlap functions and spectroscopic factors are calculated on the basis of the one–body density matrices (ODM) obtained for the nucleus ^{16}O employing different approaches to account for the effects of correlations. The calculations use the relationship between the overlap functions related to bound states of the $(A-1)$–particle system and the ODM for the ground state of the A–particle system. The resulting bound–state overlap functions are compared and tested in the description of the experimental data from (p,d) reactions for which the shape of the overlap function is important.

I. INTRODUCTION

The strong short-range and tensor components of the nucleon–nucleon interactions induce correlations in the nuclear wave function which are going beyond the independent–particle approximation, e.g., the Hartree–Fock method. Therefore it has always been a point of experimental and theoretical interest to find observables, which reflect these correlations in a unambiguous way. In this sense both, the overlap functions and single–nucleon spectroscopic factors, have attracted much attention in analyzing the empirical data from one–nucleon removal reactions, such as $(e,e'p)$, (p,d), $(d,^3He)$, see e.g. [1–4] and also in other domains of many–body physics, as e.g. atomic and molecular physics [5–12].

Recently, a general procedure has been adopted [5] to extract the bound-state overlap functions and the associated spectroscopic factors and separation energies on the base of the ground-state one-body density matrix. The advantage of the procedure is that it avoids the complicated task for calculating the whole spectral function in nuclei. One is able instead to incorporate the knowledge of realistic one-body density matrices emerging from various correlation methods going beyond the independent–particle picture which have been proposed over the years [1,13–28].

Initially, the procedure for extracting bound-state overlap functions has been applied [11] to a model one-body density matrix [29] accounting for the short–range nucleon correlations within the low–order approximation to the Jastrow correlation method (JCM). The calculations were based on a single harmonic–oscillator Slater determinant and Gaussian–like state–independent correlation functions. The resulting overlap functions have been used [30] to study one–nucleon removal processes in contrast to the mean–field approaches which account for the nucleon correlations by modifying the mean–field potentials. The results obtained for the differential cross–sections of $^{16}O(p,d)$ and $^{40}Ca(p,d)$ pick–up reactions at various incident energies demonstrated that the overlap functions can be applied as realistic form factors to evaluate absolute cross–sections of such reactions. Of course, the general success of the above procedure depends strongly on the availability of realistic one-body density matrices.

This work can be considered as an extension of the analysis of single–particle overlap functions based on the procedure [5] to more realistic one–body density matrices emerging from the correlated basis function (CBF) method [9,19,21] and the Green function method (GFM) [24]. We have chosen the CBF theory, based on the Jastrow approach [18], since it is particularly suitable for the study of the short–range correlations in nuclei. So far the calculations have been performed for infinite nuclear matter and some light nuclei as e.g. the variational Monte Carlo calculations for the ^{16}O nucleus [15]. The CBF calculations have recently been extended to medium–heavy doubly-closed shell nuclei [16,19,21,22] using various levels of the Fermi hypernetted chain (FHNC) approximation [19,20]. The Green function method [23,24] provides detailed information on the spectral functions and nucleon momentum distributions

[25,26] predicting the largest effects of the short–range and tensor correlations at high momentum and energy [27,28].

The main purpose of this work is twofold. Using the procedure [5], we first calculate all bound-state overlap functions on the basis of one–body density matrices emerging from the CBF and Green function methods for the ^{16}O nucleus in order to analyze and compare their properties in coordinate and momentum spaces. Then, the resulting overlap functions are tested in the description of the experimental data from $^{16}O(p,d)^{15}O$ reaction for which the shape of the overlap functions is important. Such an investigation allows to examine the relationship between the one-body density matrix and the associated overlap functions within the correlation methods used and also to clarify the importance of the effects of NN correlations on the overlap functions and (p,d) cross–sections.

Some basic relations of the methods used to determine the effects of correlations on the one–body density matrices are given in Section II. In Section III we present numerical results for the quantities under consideration in the case of ^{16}O. Section IV contains a summary and conclusions.

II. CORRELATED NUCLEAR WAVE FUNCTIONS

The single–particle overlap functions in quantum–mechanical many–body systems are defined by the overlap integrals between eigenstates of the A–particle and the $(A-1)$–particle systems:

$$\phi_\alpha(\mathbf{r}) = \langle \Psi_\alpha^{(A-1)} | a(\mathbf{r}) | \Psi^{(A)} \rangle, \tag{1}$$

where $a(\mathbf{r})$ is the annihilation operator for a nucleon with spatial coordinate $\mathbf{r}$ (spin and isospin operators are implied). In the mean–field approximation $\Psi^{(A)}$ and $\Psi_\alpha^{(A-1)}$ are single Slater determinants and the overlap functions are identical with the mean–field single–particle wave functions. Of course, this is not the case at the presence of correlations where both, $\Psi^{(A)}$ and $\Psi_\alpha^{(A-1)}$, are complicated superpositions of Slater determinants. In general, the overlap functions (1) are not orthogonal. Their norm defines the spectroscopic factor

$$S_\alpha = \langle \phi_\alpha | \phi_\alpha \rangle. \tag{2}$$

The normalized overlap function associated with the state α then reads

$$\tilde{\phi}_\alpha(\mathbf{r}) = S_\alpha^{-1/2} \phi_\alpha(\mathbf{r}). \tag{3}$$

The one–body density matrix can be expressed in terms of the overlap functions in the form:

$$\rho(\mathbf{r},\mathbf{r}') = \sum_\alpha \phi_\alpha^*(\mathbf{r}) \phi_\alpha(\mathbf{r}') = \sum_\alpha S_\alpha \tilde{\phi}_\alpha^*(\mathbf{r}) \tilde{\phi}_\alpha(\mathbf{r}'). \tag{4}$$

It has been shown in [5] that the one-body overlap functions (1) associated with the bound states of the $(A-1)$ system can be expressed in terms of the ground state one-body density matrix of the A nucleon system. In the case of a target nucleus with $J^\pi = 0^+$, the lowest $(n_0 lj)$ bound state overlap function is determined by the asymptotic behavior $(a \to \infty)$ of the corresponding partial radial contribution $\rho_{lj}(r,r')$ of the one-body density matrix:

$$\phi_{n_0 lj}(r) = \frac{\rho_{lj}(r,a)}{C_{n_0 lj}\ \exp(-k_{n_0 lj}\, a)/a}\ , \tag{5}$$

where the constants $C_{n_0 lj}$ and $k_{n_0 lj}$ are completely determined by $\rho_{lj}(r,r')$. In this way, both $\phi_{n_0 lj}(r)$ and $k_{n_0 lj}$ define the separation energy

$$\epsilon_{n_0 lj} \equiv E_{n_0 lj}^{(A-1)} \ - \ E_0^{(A)} = \frac{\hbar^2\ k_{n_0 lj}^2}{2m} \tag{6}$$

and the spectroscopic factor $S_{n_0 lj} = \langle \phi_{n_0 lj} \mid \phi_{n_0 lj} \rangle$. The procedure also yields the next bound state overlap functions with the same multipolarity if they exist. The applicability of this procedure has been demonstrated in Refs. [8,9,11].

Thus having the procedure for estimating such important quantities as spectroscopic factors and overlap functions one has simply to apply it to some realistic one–body density matrices emerging from the CBF and Green function methods. The latter are briefly discussed in this Section.

A. The CBF theory

The CBF theory starts from a trial many–particle wave function

$$\Psi(x_1,...,x_A) = \mathcal{S}\left[\prod_{i<j=1}^{A}\hat{F}(x_i,x_j)\right]\Phi(x_1,...,x_A), \tag{7}$$

where A is the number of the nucleons with particle coordinates $x_1, x_2, ..., x_A$ which contain spatial, spin, and isospin variables, $\mathcal{S}$ is a symmetrization operator, and Φ is an uncorrelated (Slater determinant) wave function normalized to unity and describing a closed-shell spherical system. The correlation factor $\hat{F}$ is generally written as

$$\hat{F}(x_i,x_j) = \sum_n h_n(|\mathbf{r}_i - \mathbf{r}_j|)\hat{O}^n_{ij} \tag{8}$$

with basic two–nucleon operators $\hat{O}^n$ inducing central, spin–spin, tensor and spin–orbit correlations, either with or without isospin exchange:

$$\begin{aligned} O^{n=1,...,8}_{ij} \;=\; & 1, (\boldsymbol{\tau}_i.\boldsymbol{\tau}_j), (\boldsymbol{\sigma}_i.\boldsymbol{\sigma}_j), (\boldsymbol{\sigma}_i.\boldsymbol{\sigma}_j)(\boldsymbol{\tau}_i.\boldsymbol{\tau}_j), S_{ij}, \\ & S_{ij}(\boldsymbol{\tau}_i.\boldsymbol{\tau}_j), \mathbf{L}.\mathbf{S}, \mathbf{L}.\mathbf{S}(\boldsymbol{\tau}_i.\boldsymbol{\tau}_j). \end{aligned} \tag{9}$$

The corresponding one-body density matrix

$$N(x_1,x_1') = \frac{\langle\Psi|c^\dagger(x_1')c(x_1)|\Psi\rangle}{\langle\Psi|\Psi\rangle} \tag{10}$$

has been calculated in [15] using the Monte Carlo techniques. In many cases the low–order approximation (LOA) [31–34] is used for the ODM which consists in expanding the corresponding quantities up to the first order of the function $\hat{h}(x_i,x_j;x_i',x_j') = \hat{F}(x_i',x_j')\hat{F}(x_i,x_j) - 1$. The LOA expression for the ODM is:

$$N(x_1,x_1') = N_0(x_1,x_1') + N_1(x_1,x_1') + N_2(x_1,x_1'), \tag{11}$$

with

$$N_0(x_1,x_1') = \rho(x_1,x_1'), \tag{12}$$

$$N_1(x_1,x_1') = \int dx_2 \hat{h}(x_1,x_2;x_1',x_2)[\rho(x_1,x_1')\rho(x_2,x_2) - \rho(x_1,x_2)\rho(x_2,x_1')], \tag{13}$$

$$N_2(x_1,x_1') = \int dx_2 dx_3 \hat{h}(x_2,x_3;x_2,x_3)\rho(x_1,x_2)[\rho(x_2,x_1')\rho(x_3,x_3) - \rho(x_2,x_3)\rho(x_3,x_1')]. \tag{14}$$

The zeroth order contribution (12) is the uncorrelated ODM associated with the Slater determinant Φ. An important feature of the power series cluster expansion is that sum rule properties like the normalization property is fulfilled at any order of the expansion [35]. Thus, in our case the conservation of the number of particles, i.e.,

$$\int dx_1 N(x_1,x_1) = \int dx_1 \rho(x_1,x_1) = A. \tag{15}$$

is ensured.

The overlap functions for ^{16}O have explicitly been constructed on the basis of the ODM generated by a CBF–type correlated wave function in [9]. The s.p. orbitals entering the Slater determinant Φ were taken from a Hartree–Fock calculation with the Skyrme–III effective force. The correlation factor $\hat{F}(x_1,x_2)$ obtained in [15] by variational calculations with Argonne NN forces has been used. The two–nucleon correlation factors were restricted to the central, spin–isospin and tensor–isospin operators. Such a description allows one to distinguish between the effects of different types of correlations on quantities such as overlap functions and spectroscopic factors of quasihole states.

B. FHNC formalism within the CBF theory

The CBF theory and the Fermi hypernetted chain technique have been extended in [19] to study medium–heavy doubly–closed shell nuclei in the jj coupling scheme with different single–particle wave functions for protons and neutrons using isospin–dependent two–body correlations. These are the first microscopic calculations for nuclei beyond ^{40}Ca which are a necessary step towards a correct description of heavy nuclear systems based on realistic nuclear Hamiltonian. The FHNC equations can be written in terms of the one–body densities and the two–body distribution functions:

$$\rho_1^\alpha(\mathbf{r}) = \langle \Psi^* \sum_{k=1}^{A} \delta(\mathbf{r}-\mathbf{r}_k) P_k^\alpha \Psi \rangle, \tag{16}$$

$$\rho_{2,q}^{\alpha\beta} = \langle \Psi^* \sum_{k\neq l=1}^{A} \delta(\mathbf{r}-\mathbf{r}_k) P_k^\alpha \delta(\mathbf{r}'-\mathbf{r}_l) P_l^\beta O_{kl}^q \Psi \rangle, \quad q=1,...,4, \tag{17}$$

where P_k^α is the projection operator on the $\alpha = p,n$ state of the k-nucleon. The index q labels the operational component of $\rho_{2,q}^{\alpha\beta}$ with O_{12}^q characterizing the first four channels from Eq.(9). The calculations in [19] have been performed using central nucleon–nucleon interactions (v_4) with spin and isospin dependence but without tensor and spin–orbit components:

$$v_4(1,2) = \sum_{q=1,4} v^{(q)}(r_{12}) O_{12}^q. \tag{18}$$

The structure of the FHNC equations depends on the adopted correlation function f. It has been shown in [19] that the isospin dependence of the correlation function within this approximation scheme is weak. This is due to the fact that within this approach the correlations mainly result from the central short–range components of the NN interaction. Therefore, in our calculations we use ODM for ^{16}O obtained up to the first order in the cluster expansion by adopting the Average Correlation Approximation (ACA) [19]. It consists in using of unique correlation, independent on the isospin of the nucleons. The ACA correlations are well reproduced by a sum of two gaussians:

$$f(r) = 1 - \alpha_1 e^{-\beta_1 r^2} + \alpha_2 e^{-\beta_2 (r-x)^2}, \tag{19}$$

with the parameters: α_1=0.64, β_1=1.54 fm^{-2}, α_2=0.11, β_2=3.51 fm^{-2} and x=1.0 fm. They are taken as variational parameters fixed by minimizing the FHNC ground–state energy [19]. The second ingredient of these calculations is the set of s.p. wave functions which have been generated by a mean–field potential of Woods–Saxon type.

The same s.p. wave functions but a state–dependent correlation function taken from nuclear matter FHNC calculations have been used in [21] to construct the ODM. The effects of state–dependent correlations on nucleon density and momentum distributions of various nuclei have been studied in [21]. It has been shown that the correlation functions used in these calculations lead to a general lowering of the density distributions in the interior region and to high–momentum components of the momentum distribution.

C. The Green function approach

Recent microscopic calculations of the one–body Green function for ^{16}O have demonstrated [25,26] that the nucleon–nucleon correlations induced by the short–range and tensor components of a realistic interaction yield an enhancement of the momentum distribution at high momenta. This enhancement originates from the spectral function at large negative energies and therefore should be observed in nucleon knockout reactions with large energy transfer leaving the final nucleus at an excitation energy of about 100 MeV. For a nucleus like ^{16}O with $J=0$ ground state angular momentum the one–body density matrix can easily be separated into sub–matrices of a given orbital angular momentum l and total angular momentum j. Within the Green function approach [23] the ODM in momentum representation can be evaluated from the imaginary part of the single–particle Green function by integrating

$$\rho_{lj}(k_1,k_2) = \int_{-\infty}^{\varepsilon_F} dE \frac{1}{\pi} Im(g_{lj}(k_1,k_2;E)), \tag{20}$$

where the energy variable E corresponds to the energy difference between the ground state of the A particle system and the energies of the states in the $(A-1)$–particle system (negative E with large absolute value correspond to high excitation energies of the residual system) and ε_F is the Fermi energy. The single–particle Green function g_{lj} (or the propagator) is obtained from the solution of the Dyson equation

$$g_{lj}(k_1,k_2;E) = g^{(0)}_{lj}(k_1,k_2;E) + \int dk_3 \int dk_4 g^{(0)}_{lj}(k_1,k_3;E)\Delta\Sigma_{lj}(k_3,k_4;E)g_{lj}(k_4,k_2;E), \tag{21}$$

where $g^{(0)}$ refers to the Hartree–Fock propagator and $\Delta\Sigma_{lj}$ represents contributions to the real and imaginary part of the irreducible self–energy, which go beyond the Hartree–Fock approximation of the nucleon self–energy used to derive $g^{(0)}$.

The results for the ODM have been analyzed in [24] in terms of the natural orbitals φ_α and the occupation numbers n_α in ^{16}O nucleus. Within the natural orbital representation they can be determined by diagonalizing the one–body density matrix of the correlated system. In this representation the radial ODM for each lj subspace has the form:

$$\rho_{lj}(r,r') = \sum_\alpha n_{\alpha lj}\varphi^*_{\alpha lj}(r)\varphi_{\alpha lj}(r'). \tag{22}$$

The numerical results from [24] show that the ODM can be described quite accurately in terms of four natural orbitals ($\alpha = 1,...,4$) for each partial wave lj in the sum (22). The ODM generated in this way is used in our calculations to construct the single–particle overlap functions.

III. NUMERICAL RESULTS

The ODM obtained with the different methods mentioned in Section 2 have been applied to calculate overlap functions related to the $1s$ and $1p$ states in the ^{16}O nucleus. The ODM from [9,24] account for non-central correlation effects. Therefore one obtains in these approaches different results for $p_{3/2}$ and $p_{1/2}$ quasihole states. This allows us to calculate the corresponding differential cross–sections of $^{16}O(p,d)^{15}O$ reactions leading to the ground $1/2^-$ state and $3/2^-$ excited states of the residual ^{15}O nucleus.

A. Overlap functions and spectroscopic factors

In this subsection we present the results for the overlap functions, the spectroscopic factors and the neutron separation energies calculated using the procedure of Eqs.(1)-(6) (see also [5]).

The resulting overlap functions are compared with the HF wave function in Fig. 1. The HF wave function has been calculated in a self-consistent way using the Skyrme-III interaction. It is the uncorrelated basis function, which has also been used in [9]. It can be seen from Fig. 1 that the overlap functions and the HF wave function are rather similar. This is not only true for the example of $1s$ states exhibited in this figure but also for the $1p$ hole states in ^{16}O. This justifies the use of shell–model orbitals instead of overlap functions in calculating the nucleon knock-out cross section using the Plane Wave Impulse Approximation for such kind of nuclear states. The changes in the shape from the original mean–field wave functions are rather small and might be absorbed by a suitable readjustment of the parameters of the single–particle potential used to determine the corresponding wave functions. The inclusion of short-range as well as tensor correlations leads to an enhancement of the values of the corresponding overlap functions in the interior region and a depletion in the tail region in the coordinate space. As expected, in the momentum space these effects lead to a shift of the overlap functions from the low– to the high–momentum region in comparison with the mean–field wave functions as it is shown in Fig. 2. This fact is important because the squared overlap functions in the momentum space determine the single–particle momentum distribution representing the transition to a given single–particle state of the residual nucleus. This single–particle momentum distribution can be obtained experimentally, e.g. from $(e,e'p)$ reactions, by integrating the data for the spectral function over the energy interval which includes the peak of the transition.

The values of the spectroscopic factors and the separation energies deduced from the calculations with different ODM are listed in Table 1. It is seen that the separation energies derived from ODM are in acceptable agreement with the corresponding single-particle energies obtained in self–consistent Hartree–Fock calculations. As it has been shown already in [9], the use of single-particle wave functions which

have realistic exponential asymptotics leads to separation energies of the quasihole states which are close to the original mean–field single-particle energies.

The calculated spectroscopic factors, however, differ significantly from the mean–field value. The nucleon–nucleon correlations lead to a depletion of the states which are below the Fermi level of the independent particle approach. The spectroscopic factors of the s and p states in ^{16}O obtained within the JCM (0.94 and 0.953, respectively) [11] are somewhat smaller than the values obtained from the calculations which include only central channel of the interaction (about 0.98) [9]. Although both central correlation functions have a comparable range, the first one is more effective at small r, going to zero for $r = 0$. Therefore the correlation effects induced by the central correlation function in this approach are stronger leading to a smaller spectroscopic factor. The same holds for the ODM generated in [19,21]. The comparison of the spectroscopic factors also shows that the tensor correlations, which are taken into account in [9,24], are responsible for a large part of the depletion of the occupied states. The central correlations generate a depletion of 1-2 % only, whereas the inclusion of the tensor channel leads to a depletion of 7-11 % [9]. The spectroscopic factors for the $p_{3/2}$ and $p_{1/2}$ quasihole states in ^{16}O found in [9] are about 0.90–0.91. Our calculations based on the Green function theory yield similar results which indicates that about 10 % of the $1p$–strength is removed by the short–range and tensor correlations. Here one should keep in mind that an additional depletion or reduction of the spectroscopic factors, which is not included in the approaches presented here, is due to long-range correlations [36].

In Table 1 the spectroscopic factors S are given together with the natural occupation numbers N [1] calculated after diagonalizing the corresponding one–body density matrices. The comparison shows that the results satisfy the general property $S_{nlj} \leq N_{nlj}^{max}$, i.e. in each lj subspace the spectroscopic factor S_{nlj} is smaller than the largest natural occupation number N_{nlj}^{max} [5]. The trend of the calculated spectroscopic factors follows that of the natural occupation numbers.

In the case of the Green function approach [24,25] one can compare the spectroscopic factor for the overlap function and the separation energy derived from the ODM with the occupation probability and the energy of the corresponding quasihole state listed in Table 2 of [25]. The occupation probabilities for the quasihole states (0.780, 0.898, 0.914 for $s_{1/2}$, $p_{1/2}$ and $p_{3/2}$, respectively) are slightly smaller than the spectroscopic factors listed in Table 1, indicating that the continuum contribution to the spectral function is non-negligible. The difference is largest for the $s_{1/2}$ state. The absolute energy of the quasihole state is slightly larger for the $s_{1/2}$ (34.3 MeV) than the corresponding separation energy (31.12 MeV) deduced from the ODM. In the case of the p states the quasihole energies are smaller (14.14 MeV and 17.9 MeV) than the separation energies.

B. Differential cross–sections

In order to explore whether an analysis of experimental data is sensitive to the differences in the overlap functions derived from the various many-body theories, we are now going to employ a very simple model for calculating cross–sections of $^{16}O(p,d)$ reactions. The differential cross–section for such pick–up processes can be written in the form:

$$\frac{d\sigma_{pd}^{lsj}(\theta)}{d\Omega} = \frac{3}{2}\frac{S_{lsj}}{2j+1}\frac{D_0^2}{10^4}\sigma_{DW}^{lsj}(\theta), \tag{23}$$

where S_{lsj} is the spectroscopic amplitude, j is the total angular momentum of the final state, $D_0^2 \approx 1.5 \times 10^4\ MeV.fm^3$ is the $p-n$ interaction strength in the zero–range approximation and σ_{DW}^{lsj} is the cross–section calculated by the DWUCK4 code [37]. For our purposes the standard Distorted Wave Born Approximation (DWBA) form factor has been replaced by the s.p. overlap function derived from the one–body density matrix calculations. In this case no extra spectroscopic factor S_{lsj} in eq.(23) is needed, since our overlap functions already include the associated spectroscopic factors. The results for the differential cross–sections for the transitions to the ground $1/2^-$ state and to the excited $3/2^-$ state in ^{15}O nucleus at different incident proton energies E_p=31.82, 45.34 and 65 MeV are given in Figures 3–6. A comparison with the experimental data from [38,39] is also made. The optical potentials parameter values have been taken in each case to be the same as in the corresponding standard DWBA calculations.

As can be seen in Figs.3–5 the use of all overlap functions for the transition to the ground $1/2^-$ state leads to a qualitative agreement with the experimental data reproducing the amplitude of the first maximum and qualitatively the shape of the differential cross–section. The differences between the results obtained from the various approaches are small but visible.

We emphasize that our results are without any additional normalization while the standard DWBA curves need multiplication by the fitting parameter, i.e., the spectroscopic factor. The values of the

spectroscopic factors obtained from the standard DWBA procedure are given in Table 2 and can be compared with our spectroscopic factors from Table 1. It is seen that the value of the DWBA spectroscopic factors for the $1/2^-$ state exceeds the maximum allowed value of unity.

IV. CONCLUSIONS

The results of the present work can be summarized as follows:
i) Single–particle overlap functions, spectroscopic factors and separation energies are calculated from the one–body density matrices, which were derived using different approximations to determine the correlated wave function for the ground state of ^{16}O.
ii) The overlap functions extracted from ODM calculated within the CBF and Green function theories are peaked at smaller distance in the interior region of the nucleus compared with Hartree-Fock wave functions.
iii) Considering the role of the central and the tensor correlations it is found that the correlation effects on the spectroscopic factors of the hole states are dominated by the tensor channel of the interaction.
iv) The absolute values of the differential cross–sections of $^{16}O(p,d)$ pick–up reaction at various incident energies are calculated by using the overlap functions. The resulting angular distributions are in a qualitative agreement with the experimental cross–sections of the transitions to the ground $1/2^-$ and excited $3/2^-$ states of the residual nucleus ^{15}O.

ACKNOWLEDGMENTS

The authors are grateful to Dr. G. Co' for providing us the results for ODM from [19,21] and to Dr. C. Giusti for the valuable discussions. This work was partly supported by the Bulgarian National Science Foundation under the Contracts Nrs.Φ–527 and Φ–809.

---

[1] A.N. Antonov, P.E. Hodgson, and I.Zh. Petkov, *Nucleon Correlations in Nuclei* (Springer-Verlag, Berlin, 1993).
[2] L. Lapikás, Nucl. Phys. **A553**, 297c (1993).
[3] I. Bobeldijk et al., Phys. Rev. Lett. **73**, 2684 (1994).
[4] K.I. Blomqvist et al., Phys. Lett. B **344**, 85 (1995).
[5] D. Van Neck, M. Waroquier, and K. Heyde, Phys. Lett. B **314**, 255 (1993).
[6] A.N. Antonov, M.V. Stoitsov, M.K. Gaidarov, S.S. Dimitrova, and P.E. Hodgson, J. Phys. **G21**, 1333 (1995).
[7] T. Berggren, Nucl. Phys. **72**, 337 (1965).
[8] D. Van Neck, A.E.L. Dieperink, and M. Waroquier, Z. Phys. **A355**, 107 (1996); Phys. Rev. C **53**, 2231 (1996).
[9] D. Van Neck, L. Van Daele, Y. Dewulf, and M. Waroquier, Phys. Rev. C **56**, 1398 (1997).
[10] D. Van Neck, M. Waroquier, A.E.L. Dieperink, S.C. Pieper, and V.R. Pandharipande, Phys. Rev. C **57**, 2308 (1998).
[11] M.V. Stoitsov, S.S. Dimitrova, and A.N. Antonov, Phys. Rev. C **53**, 1254 (1996).
[12] W.J.W. Geurts, K. Allaart, W.H. Dickhoff, and H. Müther, Phys. Rev. C **53**, 2207 (1996).
[13] A.N. Antonov, P.E. Hodgson, and I.Zh. Petkov, *Nucleon Momentum and Density Distributions* (Clarendon Press, Oxford, 1988).
[14] C. Mahaux and R. Sartor, Adv. Nucl. Phys. **20**, 1 (1991).
[15] S.C. Pieper, R.B. Wiringa, and V.R. Pandharipande, Phys. Rev. C **46**, 1741 (1992).
[16] G. Co', A. Fabrocini, S. Fantoni, and I.E. Lagaris, Nucl. Phys. **A549**, 439 (1992).
[17] F. Dellagiacoma, G. Orlandini, and M. Traini, Nucl. Phys. **A393**, 95 (1983).
[18] R. Jastrow, Phys. Rev. **98**, 1479 (1955).
[19] F. Arias de Saavedra, G. Co', A. Fabrocini, and S. Fantoni, Nucl. Phys. **A605**, 359 (1996).
[20] A. Fabrocini, F. Arias de Saavedra, G. Co', and P. Folgarait, Phys. Rev. C **57**, 1668 (1998).
[21] F. Arias de Saavedra, G. Co', and M.M. Renis, Phys. Rev. C **55**, 673 (1997).
[22] J.E. Amaro, A.M. Lallena, G. Co', and A. Fabrocini, Phys. Rev. C **57**, 3473 (1998).
[23] W.H. Dickhoff and H. Müther, Rep. Prog. Phys. **55**, 1947 (1992).

[24] A. Polls, H. Müther and W.H. Dickhoff, *Proceedings of Conference on Perspectives in Nuclear Physics at Intermediate Energies*, Trieste, 1995, edited by S. Boffi, C. Ciofi degli Atti, and M.M. Giannini, p.308 (World Scientific, Singapore, 1996).
[25] H. Müther, A. Polls, and W.H. Dickhoff, Phys. Rev. C **51**, 3040 (1995).
[26] H. Müther, G. Knehr, and A. Polls, Phys. Rev. C **52**, 2955 (1995).
[27] C. Ciofi degli Atti and S. Simula, Phys. Rev. C **53**, 1689 (1996).
[28] H. Müther and W.H. Dickhoff, Phys. Rev. C **49**, R17 (1994).
[29] M.V. Stoitsov, A.N. Antonov, and S.S. Dimitrova, Phys. Rev. C **47**, R455 (1993); Phys. Rev. C **48**, 74 (1993); Z. Phys. **A345**, 359 (1993).
[30] S.S. Dimitrova, M.K. Gaidarov, A.N. Antonov, M.V. Stoitsov, P.E. Hodgson, V.K. Lukyanov, E.V. Zemlyanaya, and G.Z. Krumova, J. Phys. **G23**, 1685 (1997).
[31] M. Gaudin, J. Gillespie, and G. Ripka, Nucl. Phys. **A176**, 237 (1971).
[32] M. Dal Rì, S. Stringari, and O. Bohigas, Nucl. Phys. **A376**, 81 (1982).
[33] M.F. Flynn, J.W. Clark, R.M. Panoff, O. Bohigas, and S. Stringari, Nucl. Phys. **A427**, 253 (1984).
[34] O. Benhar, C. Ciofi degli Atti, S. Liuti, and G. Salmé, Phys. Lett. B **177**, 135 (1986).
[35] S. Fantoni and A. Fabrocini, in *Lecture Notes in Physics*, Proceedings of the European Summer School on Microscopic Quantum Many Body Theories and their Applications, Valencia, 1997, edited by J. Navarro and A. Polls (Springer-Verlag, Berlin), 119 (1998).
[36] K. Amir-Azimi-Nili, H. Müther, L.D. Skouras, and A.Polls, Nucl. Phys. **A604**, 245 (1996).
[37] K. Langanke, J.A. Maruhn, and S.E. Koonin, *Computational Nucl. Phys. 2: Nucl. Reactions*, (Springer-Verlag, Berlin-Heidelberg-New York), 88 (1993).
[38] B.M. Preedom, J.L. Snelgrove, and E. Kashy, Phys. Rev. C **1**, 1132 (1970).
[39] P.G. Roos, S.M. Smith, V.K.C. Cheng, G. Tibell, A.A. Cowley, and R.A. Riddle, Nucl. Phys. **A255**, 187 (1975).

Table 1: Spectroscopic factors (S), occupation numbers (N) and separation energies (ε) deduced from the calculations with different ODM for ^{16}O

	$1s$			$1p$		
ODM	S	N	ε, MeV	S	N	ε, MeV
HF	1.000	1.000	34.89	1.000	1.000	14.84 (j=1/2)
				1.000	1.000	21.17 (j=3/2)
JCM [11]	0.940	0.950	35.82	0.953	0.965	17.48
CBF [9]	0.883	0.884	37.70	0.912	0.929	16.79 (j=1/2)
				0.909	0.917	23.30 (j=3/2)
CBF [19]	0.977	0.978	34.85	0.981	0.984	20.09
CBF [21]	0.980	0.980	34.80	0.983	0.985	20.05
GFM [24]	0.904	0.933	31.12	0.905	0.916	16.68 (j=1/2)
				0.915	0.922	20.74 (j=3/2)

Table 2: Spectroscopic factors $S_{DWBA}/(2j+1)$ deduced from the standard DWBA calculations for the $^{16}O(p,d)$ reactions leading to the $1/2^-$ ground and $3/2^-$ excited states of the ^{15}O nucleus

Proton energy, MeV	$1/2^-$	$3/2^-$
$E_p = 31.82$	1.05	0.85
$E_p = 45.34$	1.22	0.83
$E_p = 65$	1.62	0.54

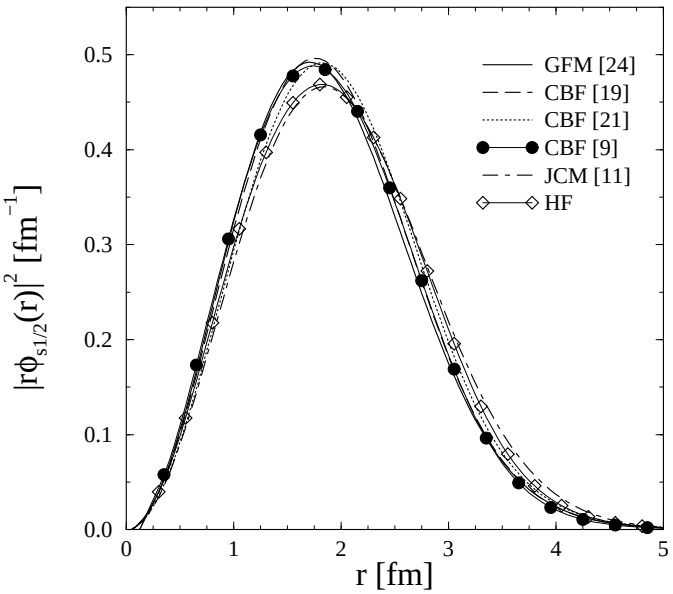

FIG. 1. Overlap functions ($r\phi(r)$ squared) for the neutron $s_{1/2}$ quasihole state in ^{16}O. All curves are normalized to unity.

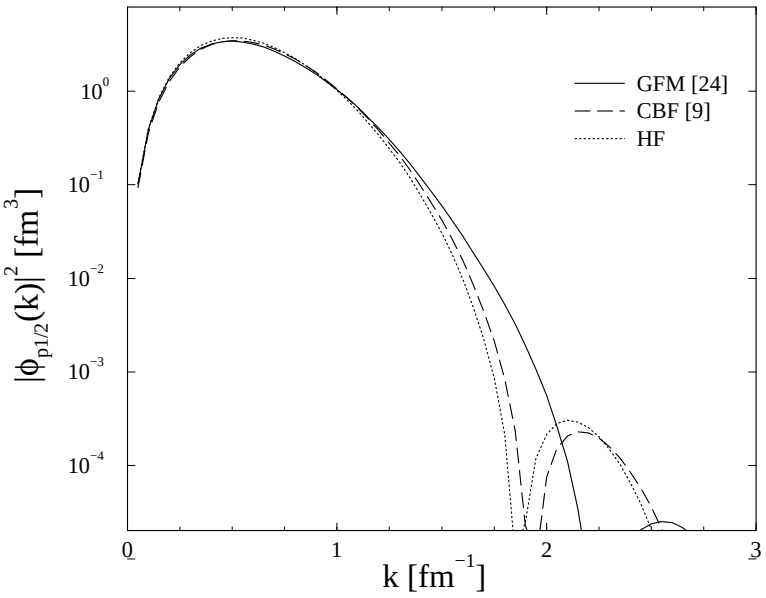

FIG. 2. Overlap functions ($\phi(k)$ squared) for the neutron $p_{1/2}$ quasihole state in ^{16}O. All curves are normalized to unity.

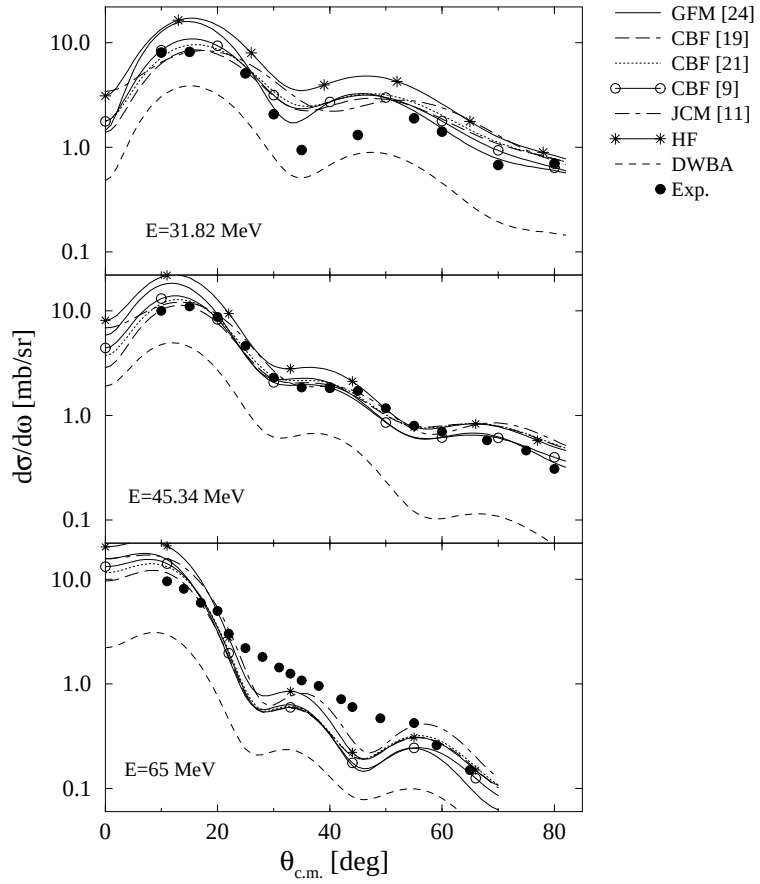

FIG. 3. Differential cross–section for the $^{16}O(p,d)$ reaction at incident proton energy $E_p = 31.82\ MeV$, $E_p = 45.34\ MeV$ and $E_p = 65\ MeV$ to the $1/2^-$ ground state in ^{15}O. The curves refering to results which are derived from various ODM are labeled by the reference, in which this ODM has been calculated. The experimental data [38] are given by the full circles.

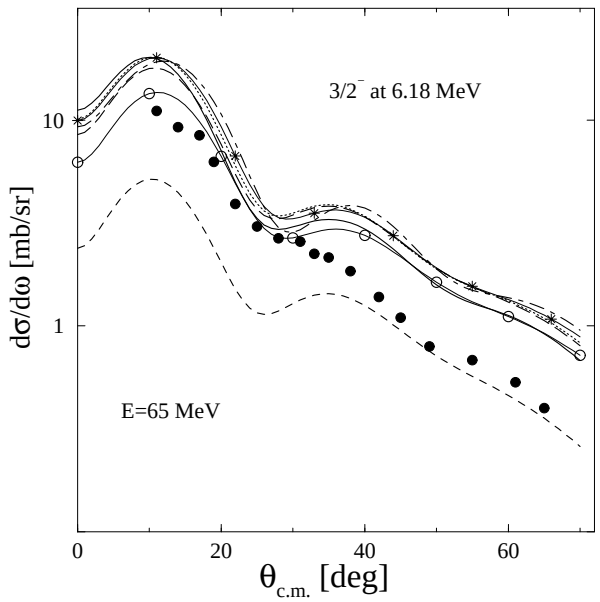

FIG. 4. Differential cross–section for the $^{16}O(p,d)$ reaction at $E_p = 65\ MeV$ incident energy to the $3/2^-$ excited state in ^{15}O. The notations are the same as in Fig.3. The experimental data are taken from [39].